



Collaborative project

Project acronym: SNM

Project full title: "**Single Nanometer Manufacturing for beyond CMOS devices**"

Grant agreement no: 318804

Deliverable: D6.5 ("Comparative study of molecular resist modification by plasma exposure")

Name of the coordinating person: Prof. Dr. Ivo W. Rangelow, Email: ivo.rangelow@tu-ilmenau.de

List of participants:

Participant no.	Participant organisation name	Part. short name	Activity Type	Country
1 (Co)	Technische Universität Ilmenau	TUIL	HER	Germany
2	EV Group E. Thallner GmbH	EVG	IND; End-user	Austria
3	IMEC	IMEC	RES	Belgium
4	Mikrosistemi Ltd	μS	SME; End-User	Bulgaria
5	Universität Bayreuth	UBT	HER	Germany
6	Technische Universiteit Delft	TUD	HER	Netherlands
7	Spanish National Research Council	CSIC	RES	Spain
8	IBM Research GmbH	IBM	IND; End-user	Switzerland
9	École polytechnique fédérale de Lausanne	EPFL	HER	Switzerland
10	SwissLitho AG	SL	SME; End-User	Switzerland
11	Oxford Instruments Nanotechnology Tools Ltd	OINT	IND; End-user	UK
12	Imperial College London	IMPERIAL	HER	UK
13	The Open University	OU	HER	UK
14	Oxford Scientific Consultants Ltd	OSC	SME	UK
15	VSL Dutch Metrology Institute	VSL	IND	Netherlands
15	University of Liverpool	ULIV	HER	UK



<p style="text-align: center;">SNM Work Package 6 Deliverable: D6.5 (“Comparative study of molecular resist modification by plasma exposure”)</p>											
Lead beneficiary number	3	Nature		R	Dissemination level		PU				
Estimated Person-months	9										
PMs by partner for the Deliverable	IMEC	OINT	OU								
	15	1	1								
Estimated Delivery Date	M36: 12/2015		Delivery Date			26/01/2016					
Author	<ul style="list-style-type: none"> IMEC vzw 										
Reviewed by:	<ul style="list-style-type: none"> WP6 Leader: J.-F. de Marneffe WPG Leader: M. Cooke Coordinator: Ivo Rangelow 										
Criteria and Achieved Results	Criteria (as described in DOW)				Achieved result						
	Comparative study of molecular resist modification by plasma exposure				More than 40 resists were compared all together, with reference to 248PR, 193PR, EUV PR and SiOC which is representative of typical HM used for pattern transfer. Line-width roughness smoothening by H2-based plasma treatments, including use of cryo-cooled process. Effect of neutral-beam plasma for resist smoothening.						



Description of the Deliverable	<p><u>DOW description:</u> <i>Comparative study of molecular resist modification by plasma exposure: Deliver comparative study of molecular resist modification by plasma exposure, benchmarked to a typical EUV resist. [month 36]</i></p> <p>PART 1: Comparative study of molecular resist modification by plasma exposure</p> <p>1.1 Introduction</p> <p>New material and process flows are being introduced, with every technological node, to realise sub-20 nm devices and follow Moore's law. The selection of these materials depends on the compatibility with the layers constituting the stack and final device purpose. For pattern transfer, a typical stack, currently used in industry, is constituted (top-to-bottom) of UV-sensitive photoresist (PR, sacrificial), hard-mask (sacrificial) and the substrate¹ (permanent). The photoresists are typically chemically amplified and tailored to be sensitive to EUV/UV optical lithography (wavelengths of 13.5, 193 and 248 nm) and achieve the target feature size or <i>critical dimension</i> (CD). In theory, besides the physical limitations of current optical lithography techniques, the smallest CD that can be achieved is equivalent to the dimensions of an individual molecule of the material composing the resist, e.g. ~5-10 nm for polymer-based photoresists². Dielectric antireflective coating (DARC), such as SiOC, is a typical hard-mask used with these photoresists. Compatibility with the lithography technique and etch selectivity w.r.t. neighbouring layers are two of the key parameters in determining the material selection. After the litho step, the SiOC hard-mask is typically etched/opened in a capacitively coupled plasma source (CCP) using fluorocarbon gases, such as CF₄.</p> <p>Various scanning probe lithography (SPL) techniques are being developed in the framework of SNM together with compatible resist materials. These techniques are non-optical and enable direct resist patterning. These resists are molecular glasses (MG) with dimensions of an individual molecule varying from a couple of nanometres down to 0.65 nm. Detailed description of the chemical properties and synthesis of these molecular glasses can be found elsewhere³.</p> <p>These MG must meet key requirements in order to be implemented. Therefore, a screening of all the MG platforms must be performed to benchmark them versus standard industrial materials. The MG performance with the various SPL techniques can be found elsewhere⁴.</p> <p>1.2 Overview of the etch performance of MG resists</p> <p>The screening and benchmarking of MG and SNM-relevant resists was performed in a CCP source using pure CF₄. The CCP chamber used in these tests was a 300mm Exelan Flex45 model from Lam research, powered through the sample holder with 2, 27 and 60MHz generator. The inter-electrode spacing was 2.34cm and the top electrode was made of Si. The wafer area pressure was regulated by computer-controller confinement rings located</p>
---------------------------------------	--

¹ SNM deliverable D6-1 figure1-2

² D. Yang et al, Journal of Material Chemistry (16), 2006, 1693-1696 DOI: 10.1039/b514146j

³ C. Neuber D-5-1 and D-5-2 SNM deliverables reports / C. Neuber et al, Proc. SPIE (9049), 2014, 90491V / C. Neuber et al, Proc. SPIE (9425), 2015, 9425E

⁴ C. Neuber, D-5-3 SNM deliverable report

under/around the top electrode. Wafers were electrostatically clamped on the table, which temperature was set to 20°C and controlled by Helium backside cooling. The upper electrode was set to 80°C. The discharge pressure was 60 mT, and was powered at 700W 27MHz RF frequency to avoid excessive ion bombardment. The selected reference materials are 193nm PR, 248nm PR and SiOC. The results of this study and etch performance are presented below. SiOC is an inorganic CVD hardmask typically used in advanced CMOS fabrication.

An overview of the etch rates (ER) of the various platforms is presented in figure 1. The materials can be divided into several groups, three containing MG-platforms and one the reference materials. The three MG resist families are UBT1-UBT5, UBT7-UBT10 and UBT11-UBT15; where UBT2, UBT8 and UBT14 are the base units of these families, respectively. Each of these groups is constituted of a fully aromatic material, the base unit, and tri-fluoromethyl or methyl-substituted aromatic materials. These resists show a slow etch rate compared to the SiOC, 193nm PR and 248nm PR. UBT11 and UBT12 exhibit a slow etch rate giving an etch selectivity of 2.8 (SiOC/resist). UBT11, UBT12 and UBT13 exhibit crystalline film formation, while UBT14 and UBT15 form dense amorphous films. UBT12 is etched almost twice as fast as UBT11, due to the existence of fluorine in its structure which induces further etch when scissioned from the parent molecule. Earlier generation of UBTx ($x < 10$, except UBT8) resists contain fluorine, nitrogen, and/or oxygen rendering them more susceptible for etch.



Figure 1: Etch rate overview of the different MG-platforms (UBTx, from UBT), Fullerene based resists (MFHM1/2 and MFPT39, from OSC), UBT/C60 mixture (from UBT/OSC), Calixarene (CM4CR, from TUIL), Polyphthalaldehyde and polydimethylglutarimide (PPA, PMGI from IBM) as well as the reference materials (SiOC, 193nm PR, 248nm PR and EUV-PR).

XPS measurements indicate an elemental change for MG-platforms where the percentage of fluorine increased after etch. Oxygen was detected after etch, even though the pristine MG platforms were O-free. Refractive index measurements, acquired by spectroscopic ellipsometry, showed a decrease of optical density as a function of etch time. FTIR measurements were also performed. However, due to the complexity of the molecules and etch mechanisms it was not possible to draw conclusions and a direct dissociation/etch of these MG-platforms.

The comparison of the surface roughness, before and after plasma exposure, of the various platforms is presented in figure 2. Most of the resists exhibit an initially low surface roughness (<0.25 nm). UBT11, 12 and 13 have a high pristine surface roughness, at least five times more than either UBT14 or UBT15, due to the crystalline nature of these films.

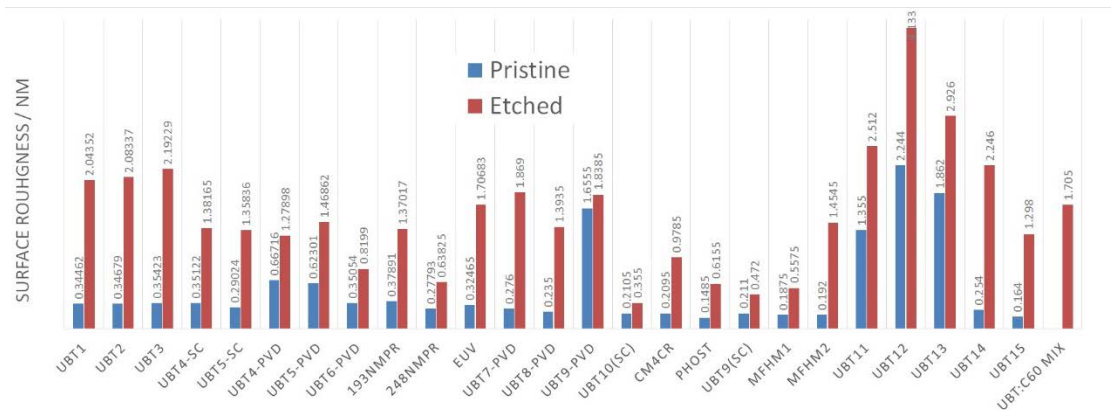


Figure 2: Surface roughness overview of the different resist platforms (UBTx) and reference materials (193nm PR, 248 nm PR and EUV-PR). The roughness is expressed in nanometer on the vertical axis.

Post applied bake (PAB) is one of many approaches used to increase the etch durability of resists. UBT8 samples were annealed at temperatures of 100°C, 175°C, 200°C and 250°C, for a duration of one minute each. Thickness measurements showed almost no change after PAB compared to that measured directly after film deposition, by PVD.

Figure 3 shows the effect of PAB on the ER of UBT8, which has a glass transition temperature (T_g) of 173°C and melting temperature (T_m) of 266°C. The etch rate of UBT8 seems to be independent of the applied bake temperature, which could be related to the high density of the material due to PVD.

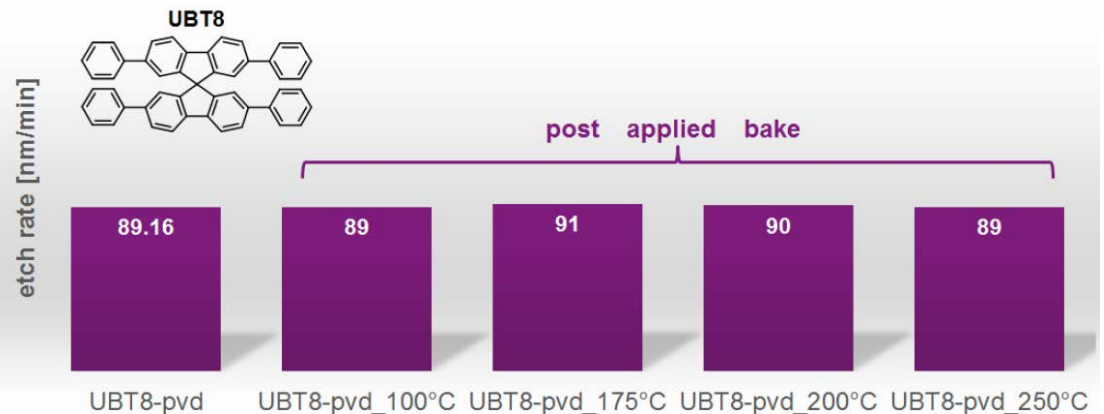


Figure 3: Etch rates of UBT8 samples after one minute of PAB at temperatures varying from 100°C up to 250°C.

In order to influence the etch durability and surface roughness of the glass resists, a mix from UBT8 and UBT14 was prepared using co-evaporation. The etch rates of pure and mixed resists are presented in figure 4. A clear increase in the etch durability can be seen for all the mixtures. The etch durability of the UBT8:UBT14 samples is almost double as that of the pure material. No clear dependency of the etch rate on the mix ratio can be currently established. Further fundamental experiments are required to explain this observed phenomenon. Using a mix of MG-platforms seems to be a promising route to improve the etch durability of these glass resists.

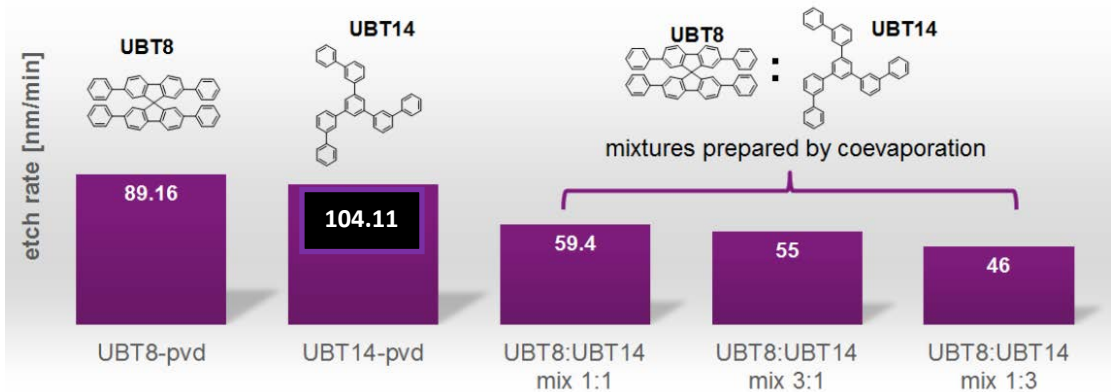


Figure 4: Etch rates of UBT8:UBT14 mixtures and the pure materials. The bar of UBT14 is not to scale as to fit all information in the figure, while the rest are.

Figure 5 shows a comparison of the surface roughness before and after etch for pure UBT8 and UBT14, PAB UBT8 samples, and UBT8:UBT14 mixture. The PAB does not seem to influence the pristine surface roughness of UBT8. However, UBT8:UBT14 (1:1 and 1:3) mixtures show an enhanced pristine surface roughness compared to the pure original materials. UBT8:UBT14 (3:1) mixture show a pristine surface roughness similar to that of UBT8. It seems that there is almost no change in the post etch roughness of annealed UBT8 samples. UBT8:UBT14 samples exhibit a small improvement of post-etch surface roughness compared to that of UBT14. Although not the same can be said compared to UBT8. Nevertheless, mixing several glass resists seems to have a positive influence on the overall etch properties of these materials.

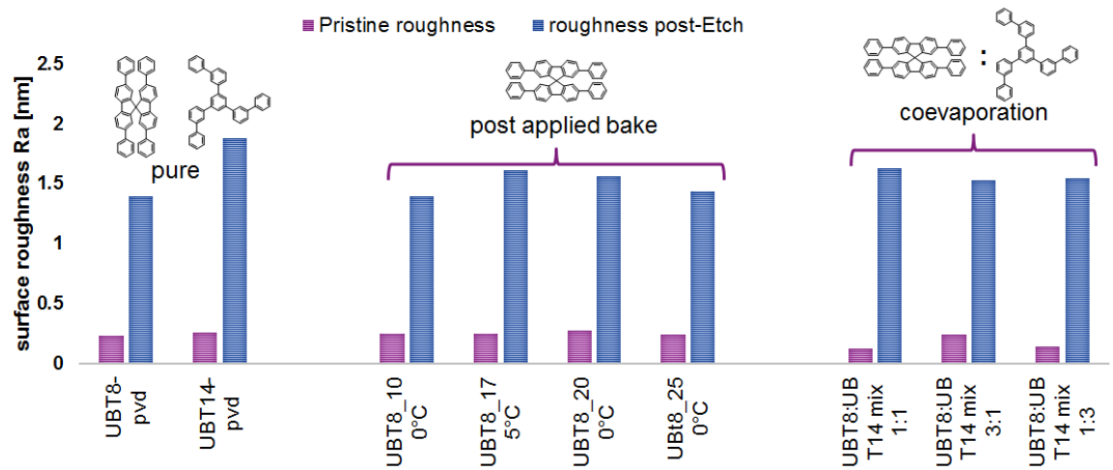


Figure 5: Surface roughness of UBT8 samples after one minute of PAB at temperatures varying from 100°C up to 250°C as well as UBT8:UBT14 mixture before (pink bars) and after etch (blue bars).

Fullerene (C60), referred to as MFHM1 and MFHM2 were supplied by OSC, were also investigated under these benchmark conditions. C60 based resist, referred to as MFHM1, showed a slow etch rate of 43.2 nm/min giving a selectivity of 4.7 (SiOC/C60). It also exhibited a very smooth surface roughness of 0.187 nm (pristine) and 0.55 nm (post-etch). The newer generation of this C60 resist, MFHM2, was also investigated. But MFHM2 exhibited a higher etch rate of 63 nm/min and surface roughness of 1.45 nm (post-etch), although it had a similar pristine surface roughness compared to MFHM1. This is attributed



to the crosslinking polymer that was used in this resist. MFPT39, which is a derivative of MFHM1, showed an etch rate comparable to that of 248nm PR. This is attributed to the added polymers that act as cross-linker and enhance the photosensitivity of this resist. This resist is more suitable for optical lithography. The addition of specific polymers to C60 resists is necessary to avoid crystallization during deposition.

C60 mixed with UBT8 was also investigated under the same conditions, see figure 1. Similarly as found for UBT8:UBT14 mixtures, the addition of C60 to the UBT8 matrix causes a massive decrease of etch rate. The surface roughness of this mixture was 0.26 nm (pristine) and 0.918 nm (post-etch), i.e. better than obtained for UBT8:UBT14 mixtures.

Calixarene (CM4CR) was also investigated and the results are shown in figures 1 and 2. Although CM4CR showed an etch rate of ~130 nm/min, it exhibited a relatively good post-etch roughness.

Polyphthalaldehyde (PPA) and PMGI (polydimethylglutarimide polymer with proprietary solvent blends, a commercial resist), were also investigated. PPA is a low dissociation temperature material used for thermal scanning probe lithography (tSPL) while PMGI is used as underlayer (heat insulator). The etch performance of PPA and PMGI under the same benchmark conditions are shown in figure 1. Both these polymers have high etch rate, with a higher removal rate for PMGI compared to PPA, which is indication that CF_4 -based chemistry might be of interest for etching PMGI with limited PPA recess. Searching for a correlation between resist etch rate and post-etch roughness, nothing clear was found.

Based on this initial screening, several resists were selected as candidates for further investigation and as candidates for nano-pattern transfer experiments. These resists are PPA (on top of PMGI), UBT8:C60 mixture and CMC4R. The selection was determined based on the performance of these resists during etching and pattern quality achieved by the various SPL techniques.

1.3 Argon Vs. CF_4 “etch”: influence on UBT6 and UBT8

The influence of physical etching (by Ar plasma) and reactive ion etching (RIE), by CF_4 plasma, was investigated on UBT6 (PHOST) and UBT8. Gel permeation chromatography (GPC) was performed on these MG-resists after plasma exposure. Several MG resists were also exposed to Ar-plasma. The “etch rate” of these resists is shown in figure 6.

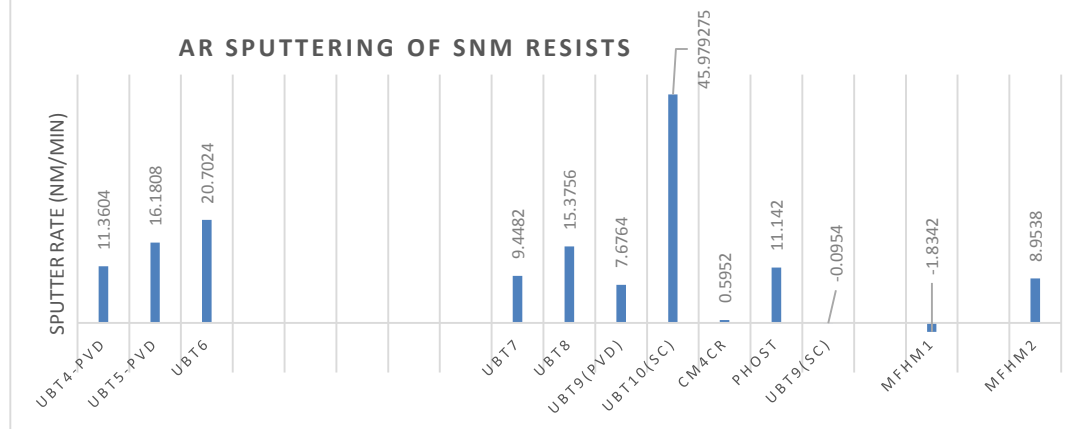


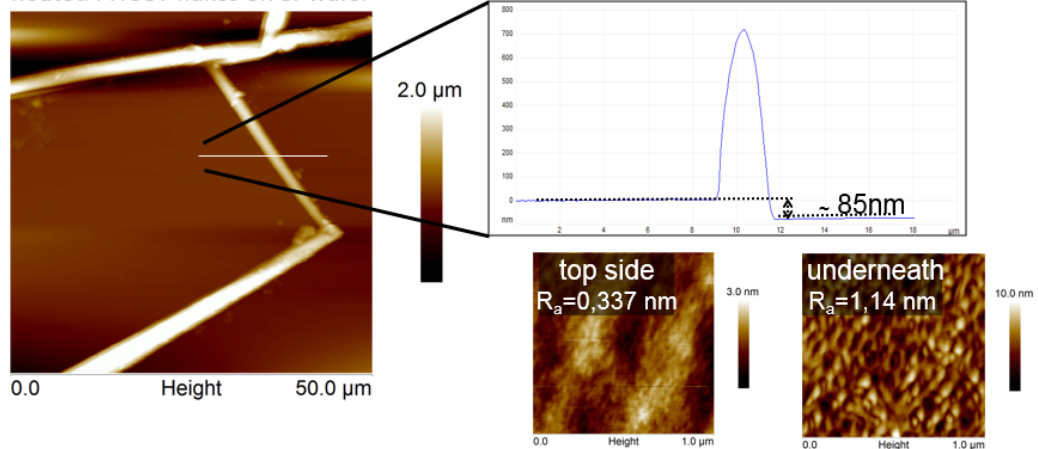
Figure 6: Etch rates (physical sputtering and/or shrinkage due to cross-linking) of selected resists exposed to argon plasma.

The decrease in thickness of these resists can be triggered by: 1) physical sputtering due to the heavy Ar ions and/or (depending on the specific resist photosensitivity) 2) cross-linking due to VUV plasma emission (Ar emitting intense lines at 104-106nm, i.e. ~ 12eV photons). The effect of the heavy ions is restricted to the resist top layer (up to a few nanometres) while the VUV can penetrate up to tens of nanometres. In RIE environment, containing fluorine, active radicals can also penetrate and diffuse through the entire layer triggering further chemical changes to the resist structure.

Figures 7-9 show the cross-linked layer thickness of UBT6 and UBT8 exposed to CF₄ and argon plasmas. UBT6, which is engineered to be photosensitive to emission in the VUV range, exhibits a complete cross-linking of the layer when exposed to argon plasma which could not be dissolved in this technique.

UBT6 (PHOST) etched in CF₄ plasma

floated PHOST flakes on Si-wafer



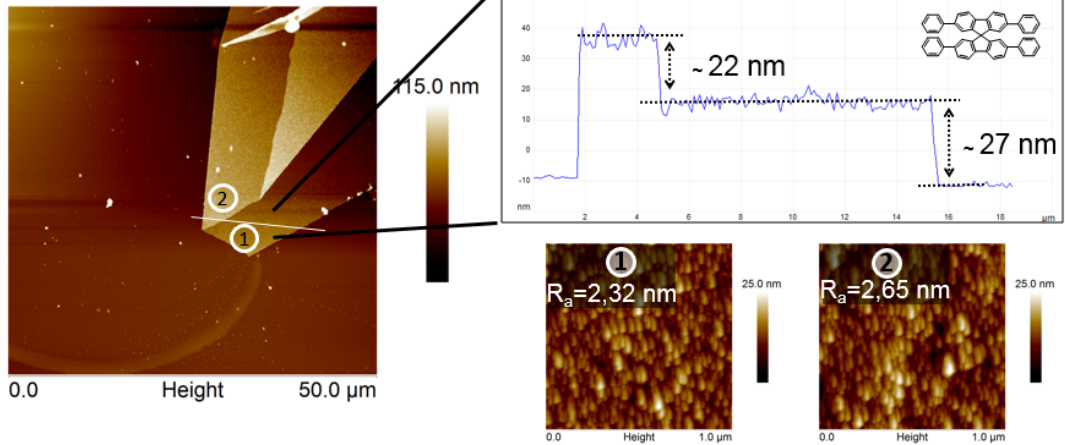
- ➔ During the CF₄ etching PHOST film is cross-linked within top layer to a depth of ca. 85 nm
- ➔ Underneath shows a clear increased area surface roughness

PHOST film prepared by spin coating, floated with PGMEA

Figure 7: Cross-linked top layer and the surface roughness of UBT6 (PHOST) after CF₄ plasma exposure.

UBT8 etched in CF₄ plasma

floated UBT8 flakes on Si-wafer

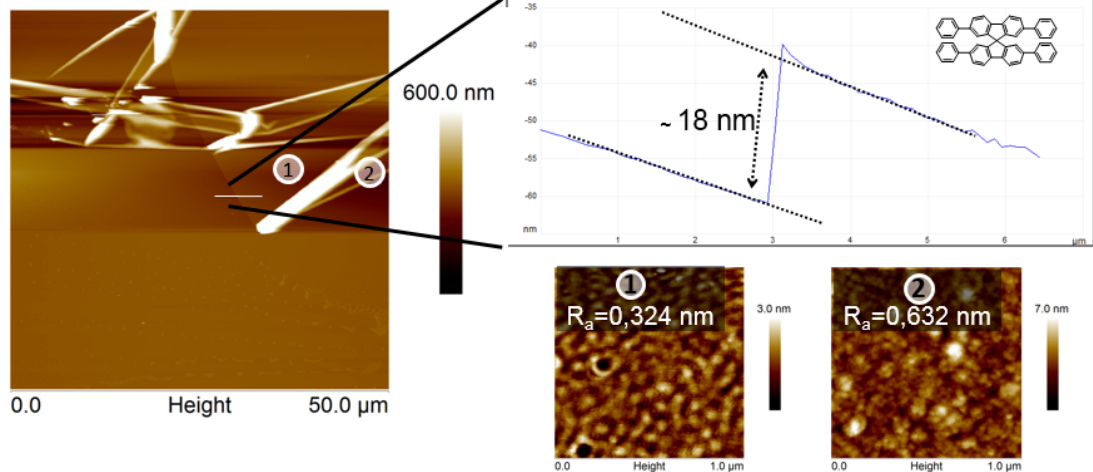


- ➔ During the CF₄ etching UBT8 film is crosslinked within top layer to a depth of ca. 25 nm
- ➔ Top side and underneath roughness are similar

Figure 8: Cross-linked top layer and the surface roughness of UBT8 after CF₄ plasma exposure.

UBT8 etched in Ar plasma

floated UBT8 flakes on Si-wafer



- ➔ During the Ar etching UBT8 film is cross-linked within top layer to a depth of ca. 18 nm
- ➔ Top side and underneath roughness are at a very low level

Figure 9: Cross-linked top layer and the surface roughness of UBT8 after Ar plasma exposure.

1.4 Conclusions

Based on the resist screening activity, a few resists have been selected to proceed with for the nano-pattern transfer tests. Also, it is important to understand the entire process flow during etching (the different steps during etching, i.e. ignition of the plasma and the de-chucking step, which is typically argon based plasma).



PART 2: LWR smoothening using H₂-based plasma

In between the SNM project submission (January 2012) and the beginning of the efforts linked to deliverable D6.5, the project requirements have evolved. Resist line-width roughness is a general problem for state-of-the-art lithography, which requires solutions to be investigated. Several approaches are typically followed to enhance the LER/LWR after lithography exposure, including PAB. Other approaches include a plasma treatment of the resist prior to etching.

The measurement of LER/LWR is challenging and the most reliable & accurate technique is by top-down CD-SEM imaging with error statistical reduction by the collection of tens of measurements per wafer. This requires the use of most advanced CD SEMs which accept only 300mm wafers. In order to complete this study within the timeframe of SNM's project, it was decided to therefore work with 300mm wafers and most advanced resists, available in large quantity, patternable over the whole 300mm surface, with high throughput and high reproducibility. As a consequence, in this part of the work, the emphasis is put on EUV resists which combine all these aspects. On-line capturing of images was performed using a Hitachi CG4000 scanning electron microscope to estimate the CD and LWR of photoresist patterns before and after plasma treatment. A set of top-view images were captured using a beam current of 8 pA and accelerating voltage of 500 V. The parameters were chosen to reduce the resist damaging while preserving the signal to noise ratio and respecting the ITRS-requirements. A rectangular scanning mode was used to acquire SEM images with a 512 x 512 pixel resolution. This mode allows us to obtain different magnifications in the x and y directions, 300 000 and 49 000 respectively with lines along the Y-direction. The field of view is 0.450 x 2.755 μm^2 giving a pixel size of 0.88 x 5.38 nm^2 . In total, 32 frames were captured. The SEM images were then analysed off-line using the Terminal PC software from Hitachi.

Although the LWR variations are within the CD-SEM's accuracy (0.3 nm 3σ for LWR and 0.6 nm 3σ for CD values), all measurements were repeated at least twice and the same LWR and CD changes were observed.

Figure 10 shows the CD and LWR changes for 22 nm lines using an industrially available EUV resist that was exposed to plasma treatment. This figure gives a summary of more than 50 treatment conditions including H₂, Ar, HBr, He and N₂ plasmas. Further details on these processes can be found elsewhere⁵.

⁵ P. De Schepper et al, Plasma Polymer and Processing 12 (2), 2014; DOI: 10.0002/ppap.201400078

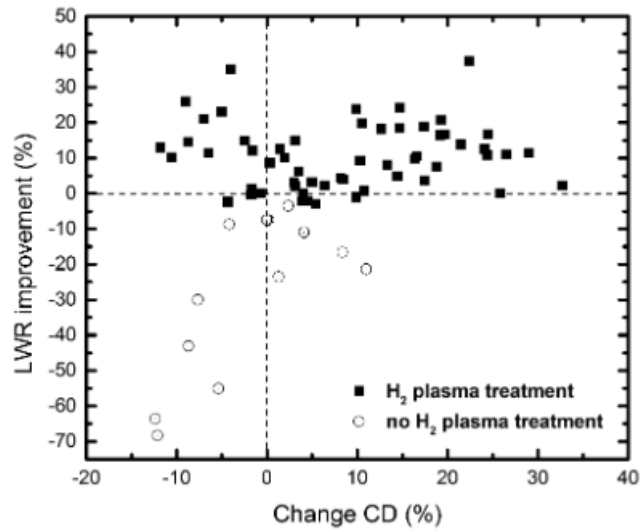


Figure 10: CD and LWR changes for 22 nm lines after plasma treatment. The data emphasizes the difference between plasma processes using hydrogen (black square) and other chemistries (open circles), including Ar, He, HBr, and N₂.

Hydrogen plasma seems to have the best LWR improvement compared to the other chemistries. The influence of the chemical composition of the resist on the LER/LWR improvement was also investigated⁶. However, figure 11 shows a comparison between the LWR improvement of some different chemistries in comparison with H₂-treatment. It can be clearly seen that hydrogen plasma treatment exhibits significant improvements.

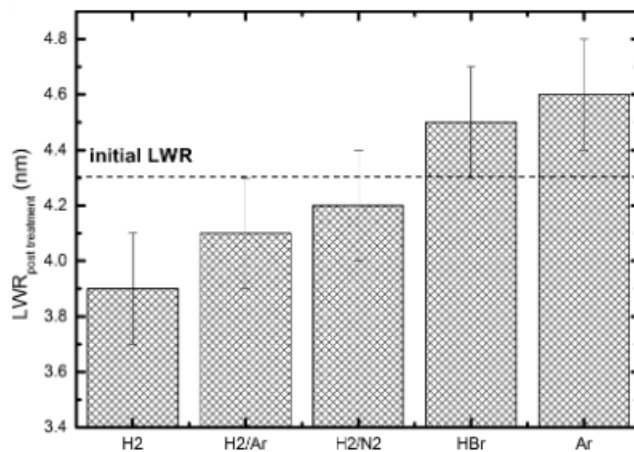


Figure 11: illustration of LWR improvement of an EUV photoresist for different plasma processes highlighting the importance of H₂ plasma treatment. The initial LWR is plotted as a dotted line and the improvement for various plasma processes is represented by the bars. 22nm ½ pitch.

The Figure 11 describes more clearly the difference between the roughness changes

⁶ P. De Schepper et al, Plasma Processes and Polymers 12 (7), 2015; DOI: 10.1002/ppap.201400157

obtained by exposing the photoresists to different kind of plasmas. For all H₂-containing plasmas, the post-plasma treatment roughness is lower than the original roughness, indicating some improvement. For pure H₂, the improvement is maximized, while mixtures of H₂ with Ar and N₂ have less effect. The HBr treatment, which is very efficient for improving LWR for 193nm resists, does not lead to any better LWR for EUV resists. For the case of Ar plasma, it is even worse.

Emphasizing on the pure H₂ plasma treatment, the Figure 12 shows the effect of plasma exposure time on the roughness, for two different EUV photoresists with different compositions (EUV A and EUV B). The FTIR spectrum of EUV A has more in common with the 193 nm acrylic based resist; while photoresist EUV B has traces from both acrylic and styrene based polymers, i.e. is a copolymer of both 193 and 248 resist backbones. Photoresist EUV B was also the best performing resist for exposure resolution of 22 nm lines. In Figure 12, it can be seen that for EUV A, the optimal treatment time for LWR improvement is around 10-20 seconds, while for EUV B it is more around 20-30 seconds. Looking at LER, in the case of EUV A there is no improvement while for EUV B there seems to be some improvement, however close to the measurement accuracy. The Figure 12 indicates that the treatment time needs to be adapted to the resist under consideration. Top down CD-SEM images confirm the reflow and smoothing capabilities of both EUV A and EUV B. After 10 seconds of plasma treatment, the reference resist A does not reflow while the LWR is reduced by 10%. However, after a process time of 30 seconds the initiated reflow is so drastic that the line width is increased by 25%. Besides this drastic reflow, the roughness is not improved any further. Unlike polymer A, photoresist B reflows already after 10s but reaches a more stable reflow rate with increasing the process time.

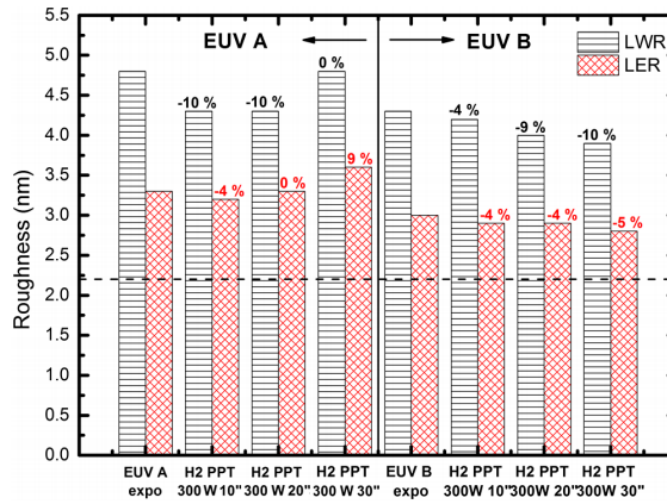


Figure 12: The influence of H₂ plasma, on LER and LWR, pre and post treatments (PPT: post-plasma treatment) for two EUV photoresists printed at 22nm ½ pitch.

In order to understand the contribution of light in the different treatments, some plasma



treatments were performed using MgF_2 and quartz optical filters covering the wafers, i.e. shading part of the light and ion/radical from the resist surface. MgF_2 has a cutting wavelength around $\sim 120\text{nm}$ while quartz has a cutting wavelength of $\sim 180\text{nm}$ – see Figure 13.

With filters, a decrease in CD with about 5% can be observed for nearly all processes. A statistical comparison between the results obtained with the two optical filters is problematic due to the measurement noise. A possible explanation for this decrease of CD is related to the interaction of the photoresist with photon emission above 170nm . For acrylate type photoresists, this photon absorption leads to side group removal that can lead to H-ablation or main chain scission and even cross linking. Removal of these functional side groups leads to “densification” and polymer rearrangement for 193 nm photoresist. Since photoresist B is an acrylate-hybrid copolymer, this densification, related to the acrylate component, is most likely responsible for the small shrinkage in CD. Even the strong emission lines around 160nm in an HBr plasma do not influence the CD. In contrast with literature, reported for 193 nm photoresist, this densification and polymer rearrangement due to UV light appears not to have a positive impact onto the line width roughness mitigation. Rather the densification itself causes slight increase of the LWR, considering a CD-SEM metrology error of about 5% of the overall roughness.

When adding the influence of the partial blocked light, photons with a wavelength at 120nm and below, and the impact of energetic radicals and ions, a large change is observed for both CD and LWR. To understand these results in detail, the plasma processes with and without H_2 and optical filters are shown in Figure 13. In the right part of the dataset for both graphs, Ar and HBr are evaluated as a smoothing process. Lines exposed to an Ar-plasma, with both strong atomic emission around 105nm and heavy Ar ions, do not show a deviation in terms of CD and LWR compared to the results obtained with only VUV emission. However, exposing the printed lines to a non-blocked HBr plasma, includes next to the H and Br related VUV emission, the reactive Br and H-species. Fully exposed, the obtained LWR seems to be less degraded compared to the influence of VUV only which is in contradiction with literature. On the other hand, the combination of VUV emission and plasma species is inducing an increase of its critical dimension. Consequently, it is crucial to understand this surprising trend. Therefore, to ease both chemical and photon induced modifications, the focus was shifted towards the more simplified H_2 plasma. The obtained results for the H_2 plasma treatment of photoresist B indicates that the synergy between the hydrogen atomic and molecular emission continuum and the reactive H_2 plasma species do influence both the change in CD and LWR. By applying 30 seconds H_2 plasma treatment, 15% “reflow” of the CD is induced. This reflow in CD can be correlated to the reduction of roughness. The plasma species that interact with the sample surface in our experiments are molecular hydrogen, hydrogen ions and atoms. Because of the low reactivity of molecular hydrogen, the hydrogen ions and atoms are expected to be the most reactive plasma species. These ions and atoms can scavenge carbon radicals simply by addition and formation of new C-H bond.

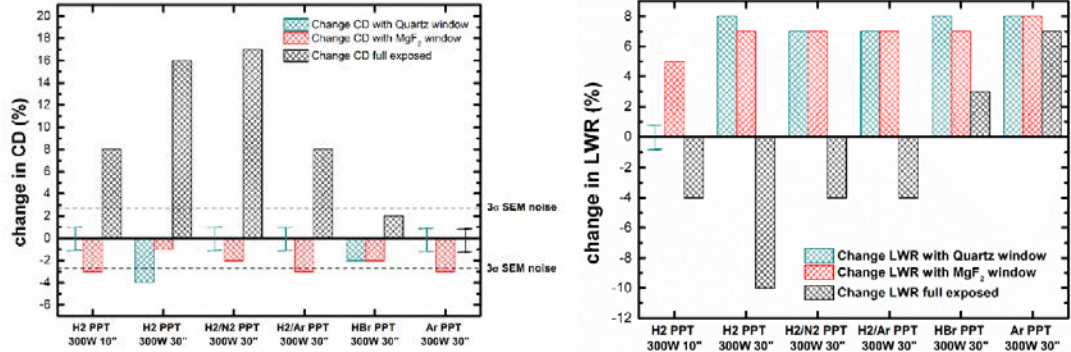


Figure 13: CD and LWR changes for various plasma exposure and filters (photoresist EUV B); 22nm ½ pitch; green and red bars indicate results obtained with the use of a quartz (green) and MgF₂ (red) optical filter which filters out the ions and radicals. (Left) change of the CD as a function of specific plasma processes. The full exposed samples (black bars) show the change of CD after exposure to photons, ions, and radicals from the plasma; (Right) Change of LWR.

It is important to understand the influence of the different species from the plasma on the LER/LWR and CD changes. This was enabled by using the plasma system developed by the Open University, Neutral Beam Etching (NBE) system, see part 4 of this report.

PART 3: Effect of process temperature during H₂ resist smoothening⁷

The sidewall roughness of resist is a key and limiting factor for pattern transfer for sub-10nm linewidth. Resist deformation, such as described in the Figure 13 above, leading to some widening of CD, can be influenced by the process temperature. Indeed, CD increase is attributed to the reflow of resist, which is determined by the glass transition temperature T_g of the backbone polymer. As this T_g can be certainly negatively influenced by the flux of heat, photons, ions radicals emanating from the plasma, cooling the wafer to sufficiently low temperature might help reducing this reflow effect.

In order to do so, wafers with EUV A resist structures, at 32nm ½ pitch (i.e. different dimension that previous paragraph, which was 22nm ½ pitch) were etched at Oxford Instruments (OINT or OIPT) for probing the low-T effect. Wafers were etched in a 300mm PlasmaLab133 ICP380 etch system. The Figure 14 shows the evolution of LWR and CD for EUV A resist treated in OIPT's PlasmaLab133 (various temperatures) and at IMEC (20°C).

⁷ This part of work generated a patent application "Plasma Method for Reducing Post-Lithography Line Width Roughness" by De Schepper Peter, de Marneffe Jean-Francois, Efrain Altamirano-Sanchez, US20150228497 A1.

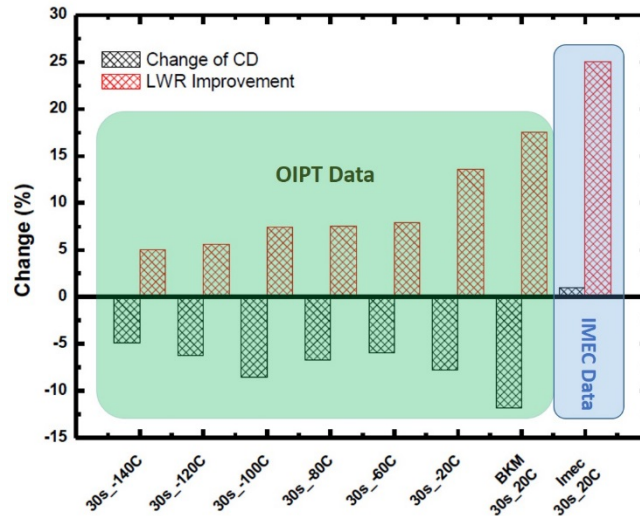


Figure 14: CD and LWR changes for 30s plasma exposure and various temperatures (photoresist EUV A); 32nm ½ pitch; green part corresponds to data recorded in OIPT’s PlasmaLab133 while blue part corresponds to IMEC’s best-known method (room temperature etch in Lam TCP Kiyo chamber). Conditions used in OIPT’s system at 20°C are copy-paste from BKM conditions used in IMEC’s system.

Comparing first OIPT’s and IMEC’s data, it appears that using identical process settings in both tools lead to different results, with major LWR improvement without CD loss in IMEC’s tool but lower LWR improvement and CD shrinkage in OIPT’s system, which is unexpected. Focusing on the impact of temperature, it appears that processing in colder conditions leads to smaller LWR improvement and smaller CD change which can be interpreted as resist becoming stiffer against plasma treatments at low T. This behaviour can be explained by looking at Figure 15.

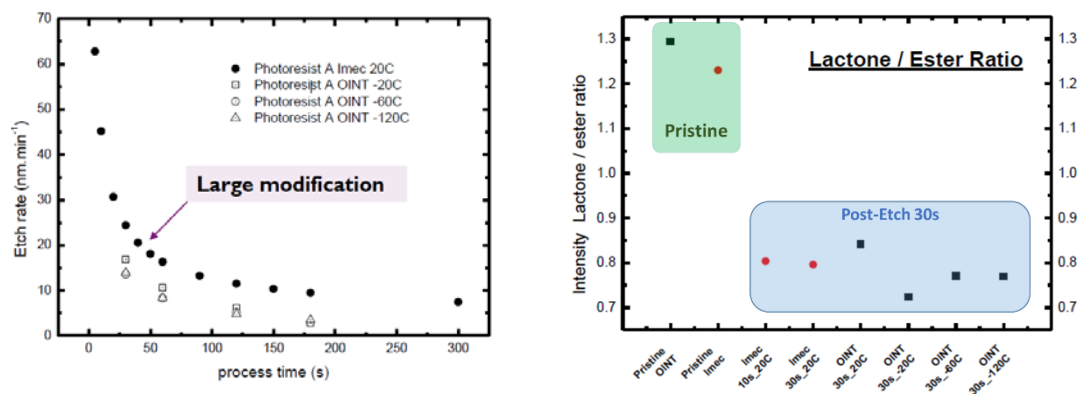


Figure 15: effect of processing wafer temperature on etch rate and lactone/ester ratio for various H₂ plasma treatments in OIPT’s PlasmaLab133 and IMEC’s Lam Kiyo chamber, for EUV A resist. Carbonyl’s C=O lactone and ester are calculated from intensities of peaks at 1800cm⁻¹ and 1735cm⁻¹ respectively.

The left-hand side of Figure 15 shows the etch rate as a function of time exposure in H₂ plasma. Similar trend is found by doing mass and refractive index measurements. A general



trend is that etch rate decreases with time, indicating some resist hardening process; typically such stiffening is related to densification, however without C=C bond formation as observed under Ar beam sputtering⁸. Lowering temperature causes a decrease of etch rate, which is also confirmed by mass measurement. The right-hand side of Figure 15 shows the evolution of carbonyl group composition, i.e. Lactone/Ester ratio for different plasma exposure and temperatures. H₂ plasma, in all conditions decreases the proportion of cyclic ester (lactone), independently of process temperature, i.e. we can conclude that temperature has negligible impact on resist chemical changes by H₂ plasma exposure. In separate work, we show that the VUV is the main contributor to LWR improvement and, at room temperature CD increase is caused by resist reflow. The origin of resist reflow is not completely understood at present. IN OIPT's case, increasing VUV flux does not cause any change in CD shrinkage meaning that VUV is not the main source of CD reflow. The main difference between the ICP (OIPT PlasmaLab133) and TCP (Lam Research Kiyō) is the distance between the plasma bulk and the wafer surface: ~ 15cm for ICP case while only few centimetres for Lam's TCP; this correlates with data from Figure 13 (left). In OIPT's ICP geometry, the wafer is therefore positioned more in the afterglow region, i.e. lower concentration of reactive species. A more likely explanation of the absence of reflow is linked to T_g, which is known to decrease as film thickness decreases⁹. As seen in Figure 15, the etch rate in OIPT's ICP chamber is much smaller in the initial stage of H₂ treatment (first 30") leading to a much lower resist recess, i.e. smaller effect on the film's T_g, which remains less prone to reflow.

PART 4: effect of neutral-beam plasma for resist smoothening

The availability of a Neutral beam source developed by Open University within WP6 of SNM's project is an opportunity to investigate the impact of neutral beam etching (NBE) and ion beam etching (IBE) for treatment of photoresists in view of roughness control and reduction. The potential advantage of the NBE/IBE technique for photoresist smoothening could serve as an exploitation route of SNM's results.

A customized reactive ion etching system (PL80 model from Oxford Instruments Plasma Technology) has been developed at OU, as shown schematically in Figure 16. The inductively coupled plasma (ICP) source of the PL80 consisted of a 3-turn coil surrounding an alumina tube of 56 mm inner diameter and 260 mm long. A grounded Faraday shield was placed between the coil and the tube to reduce capacitive coupling. Two electrodes, placed 200 mm apart, were introduced in the ICP tube for extraction of energetic particle beams. The top electrode was continuously biased with a positive voltage $0 < V_{\text{bias}} < 100$ V) while the bottom electrode was grounded. For positive ion extraction the bottom electrode was fitted with a thin stainless steel mesh (150 μm apertures and 0.32 transparency). Energetic neutral

⁸ J. J. Végh et al., Appl. Phys. Lett. 91, 233113 (2007) / DOI: 10.1063/1.2821226

⁹ J.A. Forrest et al., Phys. Rev. E 56 (5), 5705 (1997) / DOI: 10.1103/PhysRevE.56.5705

beam extraction was performed using a neutralizing graphite electrode. The transparency of the neutralizer was 0.35 with circular holes of 1 mm in diameter and 10 mm in height. Ions passing through the high aspect ratio holes have a high probability of neutralization in collisions with the sidewalls. High aspect ratio holes in the graphite neutralizing electrode can shield the UV radiation from the plasma. The substrate table was located in the diffusion region below the main plasma source and was normally grounded. The distance between the bottom electrode and the sample was 25 mm.

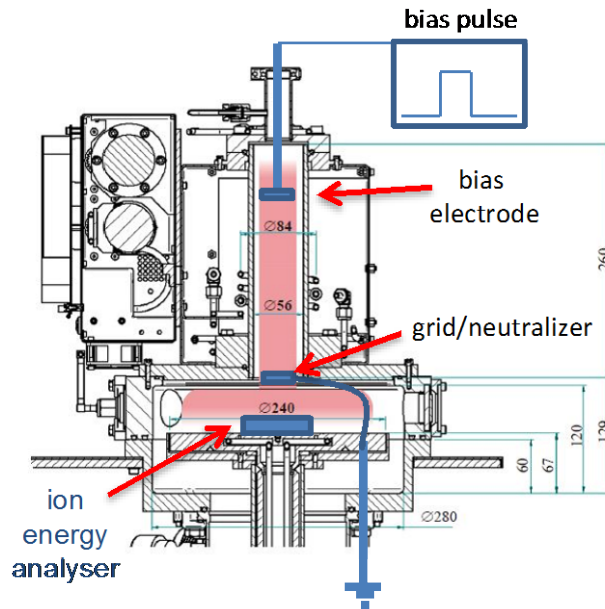


Figure 16: Schematic representation of the PL80 experimental setup. Top and bottom electrodes for energetic particle beam extraction are shown as well as Retarding Field Energy Analyser (RFEA) used for ion energy distribution probing.

The ICP was operated in pure argon and pure hydrogen in three modes:

1. Normal plasma exposure: in this mode additional electrodes were not installed and the plasma was allowed to diffuse into the sample chamber. The gas pressure in the system was fixed at $p = 30$ mTorr and the input RF power was $P = 300$ W.
2. Ion beam (IB) exposure: the bottom electrode was made of a thin stainless steel grid. The gas pressure was $p=20$ mTorr for operation in Ar and 25 mTorr for H_2 and the input RF power was $P = 300$ W.
3. Neutral beam (NB) exposure: the bottom graphite electrode with high aspect ratio holes was used. The gas pressure was $p=20$ mTorr for operation in Ar and 25 mTorr for H_2 and the input RF power was $P = 300$ W.

In this study blanket wafers were used to assess thickness and chemical changes after exposures. Patterned samples were also processed, but due to experimental limitations (the use of coupons) the LER/LWR measurements could not be performed (those require a full 300 mm wafer, while the PL80 can host only a 4" wafer). Two EUV resists, A & B, were

exposed to three different plasma configurations – see Figure 17. The first being a full plasma exposure, where all species from an ICP source reached the surface of the resist. The second configuration was exposure to ion beams (IB), where the resist interacted with directional ions (with the capability to control their energies to a certain limit) and residual VUV photons. The last configuration is the neutral beam source (NB). In this case, the energy of the energetic neutral can be controlled by the applied bias on the extractor or top plate. Also, the resist interacts only with those energetic particles, as this configuration absorbs almost up to 80% of the VUV photons. In all the last two configurations, the sample resides in the processing region which typically has two to three orders of magnitude lower pressure than that in the plasma region. Details of these system and plasma parameters can be found elsewhere¹⁰.

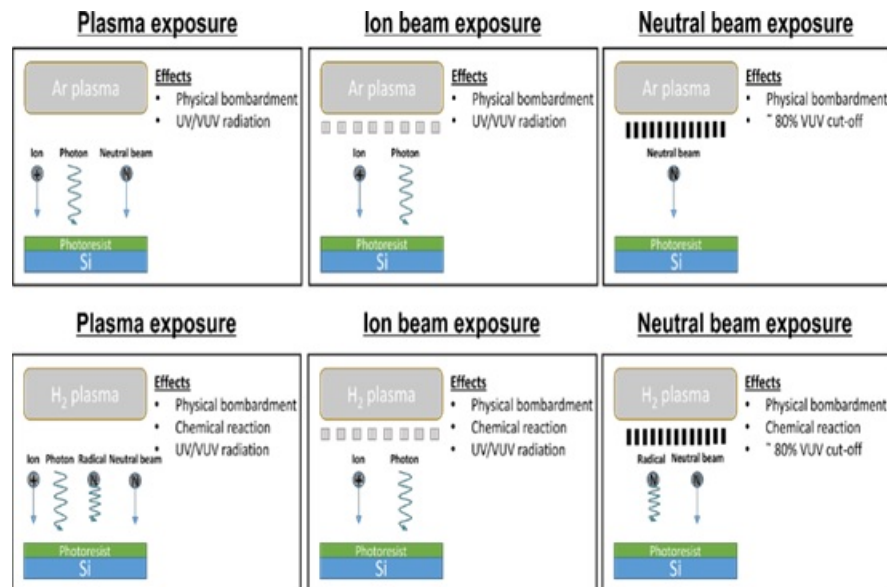


Figure 17: The schematic representation of the experimental conditions. Both Ar and H₂ plasmas, ion beams and neutral beams are used to study the effect of photons, ions and photons, and energetic neutrals.

¹⁰ D. Marinov et al., Plasma Sources Science and Technology 24 (6) 065008, 2015; DOI: 10.1088/0963-0252/24/6/065008

		Process Time (s)	Bias (V)	E _{peak} (eV)	Ion flux (10 ¹⁸ m ⁻² s ⁻¹)
Argon	plasma	100	0	6	5.7
	IB	125	0	11	1.9
		125	98	113	4.3
	NB	125	0	11	0.03
		125	98	113	0.28
H ₂	plasma	40	0	7.5	14
	IB	120	0	13	4
		120	98	113	5
	NB	120	0	13	0.1
		120	98	113	1.4

Table 1: Process conditions and corresponding peak energies and ion fluxes.

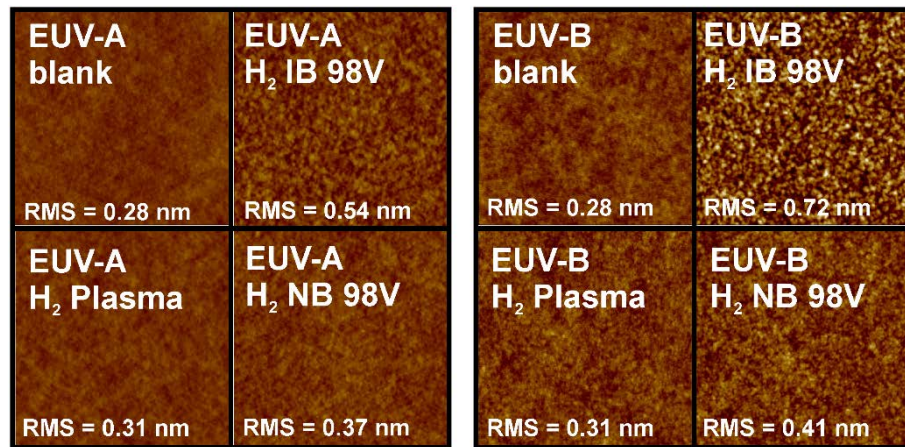


Figure 18: AFM images for both resist platforms before and after H₂ plasma treatment, including the measured RMS values

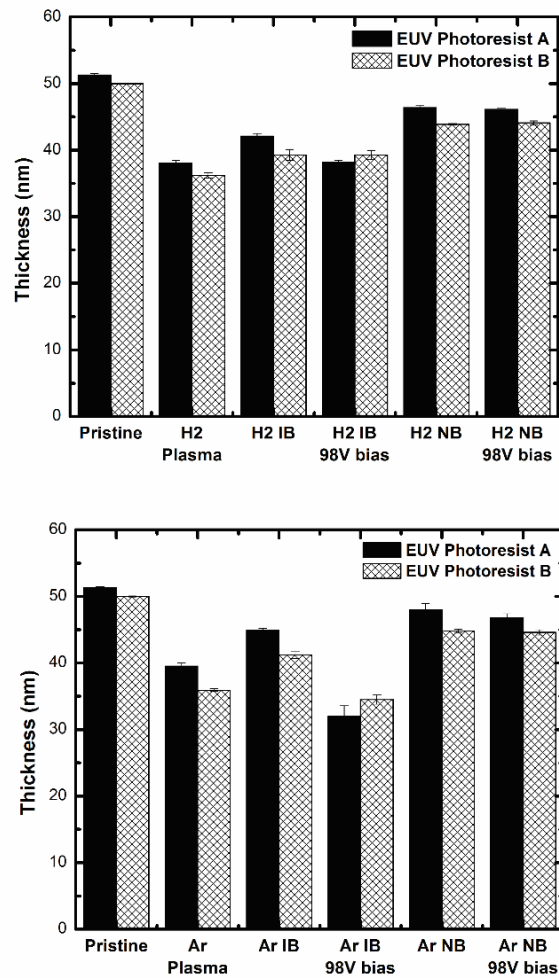


Figure 19: The thickness of EUV-A and EUV-B before and after H₂ (top) and Ar (bottom) plasma, ion and neutral interaction.

To overcome the LWR issues of present sub-30 nm patterns, we investigated how several key plasma species, such as ions, radicals and VUV photons, interact with the EUV photoresist substrate and change its line profile. Detailed results are described in a journal paper submitted for publication in *Plasma Processes and Polymers*¹¹. The work described in this paper shows both surface and bulk modifications induced by H₂ and Ar plasma, or ion and neutral beam interaction. It is found that a synergy between VUV radiation and ions with sufficient kinetic energy increases the surface roughness a little (Figure 18). However, the augmentation of the surface roughness does not seem to reach the magnitude as shown in other publications. The chemical component present within the H₂ plasma, neither the type of photoresist seem to had a significant influence. This might be related to the choice of exposure time and flux can still be of importance.

¹¹ P. De Schepper et al., *Ar and H₂ plasma and Ion/Neutral beam treatment of EUV resists*, submitted to *Plasma Processes and Polymers* (Dec. 31st, 2015)



Besides, it was shown that the interaction of only ions & neutral results in a fairly low etch rate (Figure 19), but again the reduction of overall thickness is drastically changed when adding VUV radiation. A part of this decrease is caused by the densification of the photoresist material. Also, Raman spectroscopy does not point out the formation of a top densified layer, which suggests that the penetration of the VUV photons modifies the bulk of the organic material. Consequently, FTIR shows the depletion of the carbonyl groups and subsequent chain scission after exposure of EUV1 to both H₂ and Ar. Unlike the latter, EUV-B shows similar depletion and formation of non-conjugated C=C without further chain scission. X-SEM images were included in this study as well to evaluate the impact of the various plasma components onto the resist profile. It is observed that the chemical changes, mainly induced by the VUV radiation, cause the resist lines to flow and therefore lose their profile. The authors suggest that the ester depletion and eventually chain scission induces an increased mobility and, in its way amplifies the reflow process. Finally, it can be said that the combination of physical or chemical consumption of the EUV resist, and the penetration and subsequent modification of the bulk by VUV photons causes the patterns to lose their profile.

PART 5: Conclusions

The work described in this work-package aims at 1) investigate the etch behaviour of resists synthesized and/or used by the SNM partners (IMEC activity); 2) develop a generic understanding of plasma-resist interaction (IMEC-UBT activity); 3) develop strategies towards resist smoothening (IMEC activity); and 4) explore the ability of new source configurations developed within SNM to perform resist treatments (IMEC/OU/OINT activity).

In the parts 1 & 2, the plasma resistance of all resists used in the SNM consortium have been evaluated using a reference CF₄ CCP discharge, benchmarked to non-SNM resists and materials. The quality of a resist is evaluated in terms of etch durability, post-etch roughness, crystallinity. The presence of F, N or O in the resist backbone decreases its etch resistance. The mixture of UBT8 with UBT14 or C60 improves the etch durability of the resist, however does not lead post-etch roughness below 1nm Ra which might indicate potential LER issues for fine line patterning. The PAB does not seem to influence the pristine surface roughness nor etch resistance. Looking at the combination of etch durability and post-etch roughness, no correlation is found; MFHM-1 (C60-based) shows the best of both. The presence of surface bombardment with energetic inert species (Ar⁺) lead to the formation of a heavily cross-linked surface layer which is not soluble, i.e. not washable by wet clean.

For part 3, H₂ plasma exposure is beneficial for LWR reduction for certain resists, but the process has to be carefully tailored to the plasma machine and the resist material. The mechanism is mainly driven by VUV leading to bulk modification. There is a limit which is driven by the amount of resist volume available during the H₂ smoothening process, i.e. for



	<p>small lines in the sub-10nm $\frac{1}{2}$ pitch range, the LWR gain might be inexistent. The main advantage of using low temperature ($-120^{\circ}\text{C} < T < 20^{\circ}\text{C}$) is to lower resist consumption but this at the expense of LWR gain.</p> <p>In part 4, screening various beam techniques in a single plasma system (ICP plasma, ion beam, neutral beam) allows to confirm that plasma VUV is a key element in bulk photoresist modification, leading to resist profile deformation.</p>
Explanation of Differences between Estimation and Realisation	<p><i>Precise and reproducible roughness measurement is nowadays based on CD-SEM, using statistics on hundreds of high resolution top-down images. The measurement of roughness by other methods, for instance 3D-AFM, giving capability of topographic mapping, remains challenging and with low throughput, especially for samples with densely packed nanostructures.</i></p> <p><i>Due to the unavailability of a CD-SEM capable of measuring small samples (logistics reasons), the roughness study was executed using 300mm wafer substrates. Due to practical reasons, mostly linked to amount/volume of material needed to spin-coat 300mm substrates, part of the roughness study was done on chemically amplified resist rather than SNM resists (mainly what concerns patterned resists).</i></p>